Adaptive Hybrid Spectral Methods for Stochastic Systems of Conservation Laws

Gaël Poëtte[1], Bruno Després[2], Didier Lucor[3]

[1] *CEA, DAM, DIF, F-91297 Arpajon, France,*
[2] *Laboratoire Jacques-Louis Lions, Université Pierre et Marie Curie, 75252 Paris Cedex 05, France,*
[3] *Institut Jean Le Rond D'Alembert, UMR UPMC/ CNRS 7190*
Université Pierre et Marie Curie, 4 place Jussieu, 75252 Paris Cedex 05, France.

Abstract

In this paper, we propose a new adaptive uncertainty propagation approach for systems of conservation laws, coupling Monte-Carlo and generalized Polynomial Chaos methods. Nonlinear systems of conservation laws are known for developing discontinuous solutions in finite time even for smooth initial conditions. In the context of uncertainty propagation *via* Polynomial Chaos, this aspect leads to important numerical difficulties, related to the apparition of the Gibbs phenomenon in the vicinity of discontinuities, such as treatment of the nonlinearities with loss of robustness and stability of intrusive stochastic solvers. These difficulties are not encountered when using a Monte-Carlo method for uncertainty quantification at the expense of computational cost. Our idea is then to couple the Monte-Carlo approach in the vicinity of discontinuities (as its convergence rate is independent of the smoothness of the integrand) to generalized Polynomial Chaos in the other regions (as it may provide exponential convergence rate for smooth functions). This leads to coupling different systems of conservation laws on different *physical* subdomains.

Key words: adaptive uncertainty quantification, nonlinear hyperbolic systems, conservation laws, hybrid polynomial chaos decomposition

1. Introduction

In this study, we develop *adaptive* stochastic spectral methods for nonlinear hyperbolic systems of conservation laws subject to parametric uncertainties. In this paper, we deal with uncertainty in the initial conditions of the system but the proposed methodology remains applicable to different type of uncertainties (e.g. uncertainty in the model coefficients). Uncertainty Quantification (UQ) is particularly problematic in this context because strong nonlinearities and discontinuities (e.g. shocks) associated to the compressible flow features are conveyed into the uncertain probabilistic space [27, 21, 34]. In this case, accurate approximations of the solution *via* classical Polynomial Chaos(PC)-based spectral methods fail, leading to the unwanted presence of Gibbs oscillations. The problem is particularly severe when the approximation space is constructed with polynomials based onto random variables encompassing the entire span of the underlying probability space associated with the random parameters of the system. Once the approximation space is chosen, this drawback remains no matter how the problem is solved: *i.e.* in an *intrusive* (Galerkin method) or *non-intrusive* (projection method) fashion. One way to control the oscillations with an intrusive scheme is to apply the PC decomposition technique to an *entropic* variable instead of the original prime variables of the flow [27]. This methodology is named Intrusive Polynomial Moment Method (IPMM). In this case, the weak form of the system in the stochastic approximation space of finite dimension, can be proved to remain *hyperbolic*: hyperbolicity ensures the existence of the solution and, above all, their stability in time and consequently directly impacts the stability of the numerical solution. The advantage of this approach is that it bounds the oscillations of the solution close to the shocks to a certain range through the entropy of the system without the use of any adaptive random space discretization. While very convenient, the IPMM relies on the choice of an appropriate entropic variable and also leads to a minimization step which is time consuming due to the

Email address: gael.poette@cea.fr, despres@bruyeres.cea.fr, didier.lucor@upmc.fr (Gaël Poëtte[1], Bruno Després[2], Didier Lucor[3]).

associated numerical cost.
Another way to tackle the problem, with a non-intrusive approach this time, is to *locally* increase the level of stochastic resolution necessary to bound the error [29]. This can be done, for instance, by defining a partition on the probability space which is decomposed into multi-elements within each the solution is approximated, leading to an approximation space of piecewise polynomials. For a stochastic projection method, the right balance is achieved when the aliasing error (e.g. coming from the interpolation related to the numerical quadrature) and the finite-term projection error (due to the truncation of the PC representation) are controlled to remain of comparable magnitude as the numerical error associated with the "blackbox" deterministic solver [9, 10]. Similarly to the Monte-Carlo (MC) simulation method, the advantage of this approach resides in its flexibility: there is no need to modify the deterministic solver prior to the computations and the population of solution samples may be enriched independently.
It seems therefore natural to try to combine both approaches. In [17], Ghanem already proposed an hybrid stochastic finite elements approach where he combines the versatility of MC simulation with the global convergence properties of spectral expansions for problems featuring random media. Constantine et al. [12] present a numerical method to study convective heat transfer of an incompressible flow around a cylinder subject to uncertain boundary conditions. They exploit the one-way coupling of the energy and momentum transport to derive a semi-intrusive uncertainty propagation scheme, which combines Galerkin and collocation approaches for computing statistics of the stochastic temperature field. In their case, the intrusive approach (Galerkin projection) is applied to the energy equation and the non-intrusive approach (stochastic collocation) to the nonlinear momentum equation, in two successive steps.
What we propose is different as we wish to be able to get the benefit from both approaches at the same time. Ideally, we would like to make use of the IPMM in some regions where the response of the flow to the parametric uncertainty is sufficiently smooth and resort to a non-intrusive approach to tackle regions where the flow is (possibly nonlinearly) very sensitive to the uncertainty. As the flow evolves both in space and time, we first need to *adaptively* track these regions. Then, we need to numerically insure proper interfaces between the different regions corresponding to the different UQ schemes.
In the following, we will first present the numerical method,...

2. Numerical method

In the following, we go over the adaptive hybrid numerical method that we propose. Our methodology is inspired by the recent work of Poëtte et al. [27, 25, 28, 26] who came up with a new intrusive uncertainty propagation scheme for stochastic systems of conservation laws inspired by Kinetic Theory [23, 11]. Here, the hybrid method couples both intrusive and non-intrusive techniques and can be seen as an extension of coupling methods proposed for Boltzmann/Euler equation in presence of rarefied gas [30, 31, 14, 13]. We will first explain this analogy and present the domain decomposition heuristics that adaptively sorts through the different regions of the flow. Based on this decomposition, we will present the different possible hybrid scheme combinations (but we will only focus on two [1] . We will show how we deal with numerical interfaces between adjacent regions.

2.1. *Stochastic hyperbolic system and IPMM method*

Without loss of generality, let us consider the following stochastic hyperbolic system of conservation laws in one spatial dimension.

$$\partial_t u + \partial_x f(u) = 0, u(x,t,\omega),\ x \in \mathcal{D},\ t \in]0,T[,\ \omega \in \Omega. \quad (1)$$

We define $\boldsymbol{\Xi} = \{\Xi_j(\omega)\}_{j=1}^N, N \in \mathbb{N}$, to be a $\mathbb{R}^N$-valued random array on a *probability space* $(\Omega, \mathcal{A}, \mathcal{P})$ with probability distribution $\mathcal{P}_{\boldsymbol{\Xi}}(d\boldsymbol{\xi})$, where $d\boldsymbol{\xi} = d\xi_1 \dots d\xi_N$ is the Lebesgue measure on $\mathbb{R}^N$.
We can write: $u(x,t,\omega) \approx u(x,t,\Xi_1,\Xi_2,\dots,\Xi_N) = h(x,t,\boldsymbol{\Xi})$, where $h : \boldsymbol{\xi} \mapsto h(\boldsymbol{\xi})$ is a measurable mapping from $\mathbb{R}^N \mapsto \mathbb{R}$. We will only consider *second-order* random fields, i.e. such that

$$\mathbb{E}\{\|u\|^2\} = \mathbb{E}\{\|h(\boldsymbol{\Xi})\|^2\} = \int_{\mathbb{R}^N} \|h(\boldsymbol{\Xi})\|^2 \mathcal{P}_{\boldsymbol{\Xi}}(d\boldsymbol{\xi}) < +\infty, \quad (2)$$

with $\mathbb{E}$ denotes the expectation. The random array $\boldsymbol{\Xi} \in \mathbb{R}^d$ represents the uncertainty (initial conditions, boundary conditions,...) in the system.
The projection of this system via the following multiplier $\Phi(\boldsymbol{\Xi}) = (\phi_0(\boldsymbol{\Xi}), ..., \phi_P(\boldsymbol{\Xi}))^t$ and integration with respect to the $\mathrm{d}\mathcal{P}_{\boldsymbol{\Xi}}$ measure provides a new *truncated* system:

$$\partial_t \int u\Phi \,\mathrm{d}\mathcal{P}_{\boldsymbol{\Xi}} + \partial_x \int f(u)\Phi \,\mathrm{d}\mathcal{P}_{\boldsymbol{\Xi}} = 0, \quad (3)$$

where the Φ components form an orthonormal Polynomial Chaos basis with respect to $\mathrm{d}\mathcal{P}_{\boldsymbol{\Xi}}$ [35, 18]. The system is then *closed* by use of a strictly convex *entropy* θ that insures the *hyperbolicity* nature of the truncated system.
The Intrusive Polynomial Moments Method (IPMM) consists in introducing u^P, which is implicitly imposed when the entropy

$$\Theta = \int \theta \,\mathrm{d}\mathcal{P}_{\boldsymbol{\Xi}},$$

reaches its minimum while satisfying the following constraints $(u_0, ..., u_P)^t$, solutions of (3). In the following, we will note:

$$U = \int u^P \Phi \,\mathrm{d}\mathcal{P}_{\boldsymbol{\Xi}} \text{ et } F(U) = \int f(u^P)\Phi \,\mathrm{d}\mathcal{P}_{\boldsymbol{\Xi}}.$$

[1] IPMM/MC and SPM/MC, cf. section 3.

2.2. *Analogy with coupling Kinetic Theory and Moments Theory*

In [30, 31, 14, 13], the authors are interested in numerical simulations of fluid flows with different regimes, characterized by their Knudsen number Kn. For large Kn, the regime is said rarefied (very low gas densities) and continuous hydrodynamic models (Euler, Navier-Stokes) can not describe satisfactorily the dynamics of the flow. In this case, it is wise to resort to kinetic equations [30] that are solved thanks to MC simulations DSMC for Direct Simulation Monte-Carlo, see [13] and the references therein.

Similar difficulties may be encountered with UQ based on Polynomial Chaos, especially in the context of discontinuous solutions: the resolution of truncated [2] systems can foster several difficulties [27, 25] which are not encountered when solving the stochastic partial differential equation with a non-intrusive method. Our idea is to adapt the multi-regime resolution methods used in kinetic theory to uncertainty propagation through Polynomial Chaos.

We suggest to couple the non–truncated systems (non-intrusive) with the truncated systems obtained through Galerkin Polynomial Chaos (IPMM).

2.3. *Convergence criteria heuristics and adaptive domain decomposition*

In most recent studies, researchers have recourse to adaptivity in order to alleviate the computational burden caused by the "curse of dimensionality" [6, 8, 15, 5, 16] or the long-term stability issues arising in time integration of systems with random frequencies [33]. Few others need some adaptivity in their approximation to tackle the problem of stochastic discontinuities/bifurcations often tied to some strong inherent deterministic nonlinearities [32, 4, 20].

Most of convergence criteria utilized for adaptive approaches are based on some $L^2(\Omega)$–norm of the error of the representation: for instance, in [6] the authors assess the "lack-of-fit" of the representation by means of the calculation of a linear correlation coefficient between the observations (evaluated for a non–intrusive resolution) and the polynomial surrogate model. In [24], they estimate the $L^2(\Omega)$–norm error of their representation (non–intrusive resolution) in order to identify the best random direction to refine (anisotropic Smolyak numerical quadrature). The convergence may be based on the statistics of the solution as well. In [34], the contribution of additional expansion terms to the variance within each local element of the partition of the parametric space is quickly evaluated thanks to the hierarchical nature of the gPC expansion.

[2] Note that in this paper, we do an important distinction between truncated/non–truncated *systems* and intrusive/non intrusive *methods*: the first refers to the systems we want to couple in this paper. The second refers to the resolution methods used in order to numerically accomplish the coupling.

For our coupled algorithms, we propose to use a simple criteria $\varepsilon^P(x)$, varying in space and for fixed time, based on the absolute value of the remainder of the stochastic polynomial chaos expansion:

$$\varepsilon^P(x) = \left| \sum_{k=P+1}^{\infty} u_k(x,t)\Phi_k \right|. \tag{4}$$

In practice, the remainder is computed to check the convergence of the expansion coefficients: we consider that the solution has converged if $|u_{P+1}| < \varepsilon^P$. Otherwise, the polynomial order and/or the number of points is/are incremented if the expansion does not satisfy the criteria.

Let us introduce the function h such that [3]

$$\begin{cases} h(x) = 0, & \text{for } x \in \mathcal{D}\backslash\mathcal{D}_N, \\ h(x) = 1, & \text{for } x \in \mathcal{D}_N. \end{cases} \tag{5}$$

The function h is defined equal to one in a "validity" domain of the truncated system, based on a notion of "equilibrium of the distribution u^P and zero elsewhere. The results are generalizable to the case of a smooth function (see [14]).

Definition 2.1 (Equilibrium of u^P) *The distribution u^P is said at equilibrium if the parameter $\varepsilon^P(x)$ is close to zero for $x \in \mathcal{D}$ fixed. It is implicitly defined by verifying the following conditions*

$$\begin{aligned} &\lim_{P \longrightarrow \infty} \varepsilon^P(x) = 0, \forall x \in \mathcal{D}, \\ &\text{For fixed } P < \infty, \exists\, x \in \mathcal{D} \text{ such that } \varepsilon^P(x) = 0, \\ &\lim_{\varepsilon^P \longrightarrow 0} u^{\varepsilon^P} \longrightarrow u^P_{eq}, \end{aligned}$$

where u^{ε^P} denotes the solution of the non–truncated system (1) and u^P_{eq} denotes the solution of the truncated system (3).

This definition echoes the notion of thermodynamical equilibrium in kinetic theory.

Several choices are possible for the explicit definition of $\varepsilon^P(x)$. This question will be tackled later in this paper.

Remark 2.3.1 *In kinetic theory, Kn allows the characterization of the thermodynamical equilibrium: the more it tends to zero, the more the density of presence of the particles f^ε tends to thermodynamical equilibrium. In other words, in the limit $Kn \longrightarrow 0$, the moment equations (verified implicitly by f^ε) are valid. In the context of coupling intrusive and non-intrusive methods, ε^P plays the role of Kn for our UQ method.*

Function h can also be defined *via* $\varepsilon^P(x)$: at fixed $P < \infty$ as,

$$\begin{cases} h(x) = 0, & \text{if } \varepsilon^P(x) \longrightarrow 0, \\ h(x) = 1, & \text{elsewhere.} \end{cases} \tag{6}$$

[3]

We then consider that our vectors of uknowns explicitly depends on ε^P: u^{ε^P} and U^{ε^P}. When $\varepsilon^P \longrightarrow 0$, u^{ε^P} tends to equilibrium $u^P_{eq} = \nabla_\lambda \theta^*(\Pi^P v)$ solution of (3).

The function h decomposes $\mathcal{D}$ in several subdomains: we denotes by $\mathcal{D}_N = \{x \in \mathcal{D} : \varepsilon^P(x) \longrightarrow 0\}$ and by $\mathcal{D} \setminus \mathcal{D}_N$ its complementary. In the following sections, we go over the systems solved on each sides of the interfaces defined through h. We explain in which sense these coupled systems are consistent with the resolution of the system (1). Let us consider three possible configurations between two regions (non–truncated/non–truncated, truncated/truncated and non–truncated/truncated) and let us specify the boundary conditions between these regions.

2.4. *Coupling algorithms*

In the following, we refer to the Spectral Projection Method (SPM) as the non-intrusive method that approximate the stochastic solution by projecting it directly onto each member of the chosen approximation space. This Galerkin projection involves multi-dimensional integrals that can be evaluated through numerical quadratures.

2.4.1. *The different Hybrid system schemes*

The non–truncated system is the system we want to solve in the whole computational domain $x \in \mathcal{D}$, with time $t \in]0, T[$. A direct calculation by MC simulations is not possible due to its slow convergence rate and to the cost of one deterministic computation of the non–truncated system. We suggest a new coupling method between the non–truncated system (MC, SPM, collocation) and the truncated system from IPMM.

The coupling method we suggest is an adaptive PC based method inspired of [14]. It consists in the resolution of the non–truncated system in certain regions of the simulation domain $x \in \mathcal{D}_N \subset \mathcal{D}$ and of the non–truncated system in the complementary region $\mathcal{D} \setminus \mathcal{D}_N$. We emphasize that this work focuses on the adaptive decomposition of the physical computational domain $\mathcal{D}$ rather than the stochastic domain Ω [1, 21, 22, 34, 2]. The decomposition of $\mathcal{D}$ in subdomains is directly linked to the choice of the heuristic. In the following sections, we describe the models we solve in the different subdomains and suggest a simple criteria enabling the decomposition of $\mathcal{D}$. The following section is inspired of [14, 13].

2.4.2. *Hybrid non–truncated-non–truncated system scheme*

We define the left distribution $u^{\varepsilon^P}_G = h u^{\varepsilon^P}$ and right distribution $u^{\varepsilon^P}_D = (1-h) u^{\varepsilon^P}$ and we verify they satisfy the systems

$$\partial_t u^{\varepsilon^P}_G + h \partial_x f(u^{\varepsilon^P}_G + u^{\varepsilon^P}_D) = 0, \tag{7}$$

$$\partial_t u^{\varepsilon^P}_D + (1-h) \partial_x f(u^{\varepsilon^P}_D + u^{\varepsilon^P}_G) = 0. \tag{8}$$

The initial conditions of (7)-(8) are given by $u^0_G = h u^0$ and $u^0_D = (1-h)u^0$, if u^0 denotes the initial condition of (1). This leads to the following properties (inspired by [14]):

Property 2.4.1 *If $(u^{\varepsilon^P}_G, u^{\varepsilon^P}_D)$ is the solution of problem (7)-(8) with initial conditions (u^0_G, u^0_D), then $u^{\varepsilon^P} = u^{\varepsilon^P}_G + u^{\varepsilon^P}_D$ is solution of (1) with initial condition u^0. The reciprocal property is also true.*

Proof The results are immediate. ■

Remark 2.4.1 *Note that the last property implies that, through the suggested UQ coupling method, we will be able to couple non-intrusive methods with different levels of resolutions and /or different kinds of quadrature rules in the different subdomains.*

2.4.3. *Hybrid non–truncated-truncated system scheme*

We suppose the right region is at equilibrium (i.e. the truncated equations are "valid"): we look for the approximation of (8) when $\varepsilon^P \longrightarrow 0$. On the left hand side of the interface, the non–truncated system (7) (only) is valid.

Property 2.4.2 *When $\varepsilon^P \longrightarrow 0$, $u^{\varepsilon^P}_D$ tends to the solution $u^P_{eq} = \nabla_v s^*(\Pi^P)$ whose moments verify the truncated system*

$$\partial_t U^{\varepsilon^P}_D + (1-h)\partial_x \left[\int f(u^P_{eq} + u^\varepsilon_G) \Phi \mathrm{d}\mathcal{P} \right] = 0. \tag{9}$$

Proof By taking the moments of (8), we obtain:

$$\partial_t U^{\varepsilon^P}_D + (1-h)\partial_x \left[\int f(u^{\varepsilon^P}_D + u^\varepsilon_G) \Phi \mathrm{d}\mathcal{P} \right] = 0. \tag{10}$$

As $\varepsilon^P \longrightarrow 0$ in this latter expression, we obtain the results. ■

This last property helps to define the boundary conditions between the two subdomains: the coupled model system non–truncated/truncated can be written

$$\partial_t u^{\varepsilon^P}_G + h \partial_x f(u^{\varepsilon^P}_G + u^P_{eq}) = 0, \tag{11}$$

$$\partial_t U^{\varepsilon^P}_D + (1-h)\partial_x \left[\int f(u^P_{eq} + u^\varepsilon_G) \Phi \mathrm{d}\mathcal{P} \right] = 0. \tag{12}$$

The initial conditions are given by $u^0_G = h u^0$ and $U^0_D = (1-h)U^0$. Then, the solution to problem (1) is given by $u^{\varepsilon^P} = u^{\varepsilon^P}_G + u^P_{eq}$ such that $u^{\varepsilon^P}_G$ is the solution on the left u^P_{eq} is the solution on the right.

2.4.4. *Hybrid truncated-truncated system scheme*

As in the precedent subsections, we show that when both domains on each sides of the interface are at "equilibrium", the coupling method enables to find back the truncated system (3).

Property 2.4.3 *When $\varepsilon^P \longrightarrow 0$, the moments of $(u^{\varepsilon^P}_G, u^{\varepsilon^P}_D)$, solutions of (7)-(8), denoted by $(U^{\varepsilon^P}_G, U^{\varepsilon^P}_D) =$*

$(hU^{\varepsilon^P}, (1-h)U^{\varepsilon^P})$, *converge to the solutions* (U_G, U_D) *of the truncated systems*

$$\partial_t U_G + h\partial_x F(U_G + U_D) = 0, \tag{13}$$

$$\partial_t U_D + (1-h)\partial_x F(U_D + U_G) = 0. \tag{14}$$

with the initial conditions $U_G^0 = hU^0, U_D^0 = (1-h)U^0$. *Besides,* $U = U_G + U_D$ *is solution of* (3).

Proof The proof is similar to the proofs of properties 2.4.1 and 2.4.2: it is enough taking the moments of (7) and (8) and considering that ε^P tends to 0 in the obtained systems. The sum of the obtained systems shows that $U = U_G + U_D$ is solution of (3). ■

Remark 2.4.2 *Note that the last property implies that, through the suggested UQ coupling method, we will be able to couple intrusive methods with different levels of resolutions and different entropies in the different subdomains: Low polynomial order on the left and higher polynomial order on the right for example or the use of different entropies on each sides: indeed, we have seen [27] that taking* $\theta(u) \neq \frac{u^2}{2}$ *as a closure entropy implies a supplementary cost (minimization algorithm) but is relevant and accurate in the vicinity of discontinuities. This point will be tackled in further publications.*

2.5. *Coupling systems* $\Longrightarrow$ *Coupling stochastic resolution methods*

In this section, we describe the coupling algorithm more practically. The resolution of the coupling between the non–truncated and truncated systems leads to the coupling of the resolution methods of these systems: we present the new uncertainty propagation method coupling intrusive and non-intrusive methods on one time step. We illustrate it in the case of a coupling between non–truncated (left) and truncated (right) systems, the other possible combinations results from the same kind of manipulations. The talk is illustrated by table 1.

At the begin of the time step, the heuristic is tested and new areas $\mathcal{D}_N$ and $\mathcal{D} \setminus \mathcal{D}_N$ are defined.

Suppose $\mathcal{D}_N$ is on the left hand side of the interface defined by h (through ε^P). On the left hand side of the interface, we want to solve the non–truncated system (11): we turn to a non-intrusive method [4]. Let's choose N points, $(\xi_i)_{i\in\{1,...,N\}}$ with associated weights $(w_i)_{i\in\{1,...,N\}}$. In this subdomain, $\varepsilon^P \nrightarrow 0$ so that $h(x) = 1$ for $x \in \mathcal{D}_N$. Equation (11) simplifies to

$$\partial_t u_G^{\varepsilon^P} + \partial_x f(u_G^{\varepsilon^p}) = 0. \tag{15}$$

the resolution of (15) implies the resolution of N decoupled systems

$$\begin{aligned}
&\partial_t u_G^{\varepsilon^P}(x,t,\xi_1) + \partial_x f(u_G^{\varepsilon^p}(x,t,\xi_1)) = 0,\\
&\qquad\qquad ...\\
&\partial_t u_G^{\varepsilon^P}(x,t,\xi_i) + \partial_x f(u_G^{\varepsilon^p}(x,t,\xi_i)) = 0,\\
&\qquad\qquad ...\\
&\partial_t u_G^{\varepsilon^P}(x,t,\xi_N) + \partial_x f(u_G^{\varepsilon^p}(x,t,\xi_N)) = 0.
\end{aligned} \tag{16}$$

In $\mathcal{D}\setminus\mathcal{D}_N$, we want to solve the moment system (12) (truncated). In this domain, the solution is at "equilibrium": $\varepsilon^P \longrightarrow 0 \Longrightarrow h(x) = 0, \forall x \in \mathcal{D}\setminus\mathcal{D}_N$ so that (11) simplifies to

$$\partial_t U_D + \partial_x \left[\int f(u_{eq}^P)\Phi \mathrm{d}\mathcal{P} \right] = 0. \tag{17}$$

The system (17) is solved thanks to an intrusive method. Once again, the choice of the intrusive resolution method in $\mathcal{D}\setminus\mathcal{D}_N$ is free: it is enough choosing the basis of multiplicators $(\phi_0, ..., \phi_P)^t$ (polynomials [27], piecewise polynomials [34], wavelets [21],...) with a closure entropy $\theta(u)$ defining the form of the equilibrium distribution $u_{eq}^P = \nabla_\lambda \theta^*(\Pi^P \lambda)$.

Now remains to define the boundary conditions in each regions $\mathcal{D}_N$ and $\mathcal{D} \setminus \mathcal{D}_N$: the results are presented in table 1.

– In domain $x \in \mathcal{D}_N$, the moments of $u_G^{\varepsilon^P}$ at the boundaries of $\mathcal{D}_N$ are evaluated from the solution taken at the points $(\xi_i)_{i\in\{1,...,N\}}$:

$$\begin{aligned}
U_{Boundaries}(x,t) \approx \sum_{i=1}^{N} w_i u_G^{\varepsilon^P}(x,t,\xi_i)\Phi(\xi_i)\\
\forall x \in \partial\mathcal{D}_N \text{ and at fixed } t.
\end{aligned} \tag{18}$$

In practice, we use a ghost cell in $\mathcal{D}_N$ for the computation of the fluxes from $\mathcal{D}_N$ to its neighboor area.

– For $x \in \mathcal{D} \setminus \mathcal{D}_N$, the moments implicitly define the equilibrium distribution $u_{eq}^P(x,t,\xi)$. This distribution enables to compute the punctual values at the boundaries of $x \in \mathcal{D} \setminus \mathcal{D}_N$:

$$\begin{aligned}
\forall i \in \{1,...,N\},\ u_{Boundaries}(x,t,\xi_i) \approx u_{eq}^P(x,t,\xi_i)\\
\forall x \in \partial(\mathcal{D} \setminus \mathcal{D}_N) \text{ and at fixed } t.
\end{aligned} \tag{19}$$

Once again, in practice, we resort to ghost cells enabling the computation of the fluxes form $\mathcal{D} \setminus \mathcal{D}_N$ to its neighboor area.

Remark 2.5.1 *Note that the well-posedness of the coupled systems (even if they are both well posed (hyperbolic here) has not been proved and constitutes an open problem [3, 7]. A more theorical study of the method will be tackled in further publications.*

3. Numerical results

In this section, we apply the new coupling uncertainty propagation method to two different equations. First Burg-

[4] We recall that the coupling we describe here leave the choice of the non-intrusive and intrusive method in the different regions.

ers' equation: it is a scalar equation which present the advantage of having analytical solution and consequently to compare the accuracy of the different methods applied. We then consider the case of Euler system in 1-D cartesian coordinates.

The coupling approach allows many combinations amongst the coupling of systems [5] as well as methods [6]. We can not present all the results obtained for all possible combinations in this paper. They are under study and will be the purpose, for the most efficient, to further publications. In this paper, we suggest to focus on two different simple combinations in order to give a hint of the efficiency and capacity of the approach.

In every numerical results presented in this section, the selected heuristic consists in a test on the last coefficient of the polynomial chaos development of the vector of unknowns $u_{P_{low}}$:

$$\begin{cases} h(x,t) = 0, & \text{if } u_{P_{low}}(x,t) < \varepsilon_{threshold}, \\ h(x,t) = 1, & \text{elsewhere.} \end{cases} \tag{20}$$

In practice, we choose the threshold $\varepsilon_{threshold} = 10^{-8}$ in the next simulations

3.1. *Stochastic inviscid Burgers equation*

The methodology previously described is applied to the simple case of a stochastic scalar conservation law: the inviscid Burgers equation with uncertain initial condition. We consider a stochastic initial condition described by two *iid uniform* random variables to represent exactly the random initial condition.

We suggest to reconsider the test-case IC_3 presented in [27] for Burgers equation:

$$\partial_t u + \partial_x \frac{u^2}{2} = 0, x \in \mathcal{D} = [0,1], t \in [0, 0.55]. \tag{21}$$

We refer to [27] for more details on the physical relevance, the mathematical and analytical solutions and the expression of the truncated system. The problem involves two shocks whose uncertain magnitudes reflect in the stochastic domain. Initially, the shocks are far from each others (see figure 3 top left or 1 left). As time passes, the second shock goes faster than the first one and reaches it, interacts with it, see figure 1 right. This can lead to very complex patterns in the stochastic domain, at some specified locations, as time passes, see figure 2 (left) where the shocks are interfering with each others at this time and location.

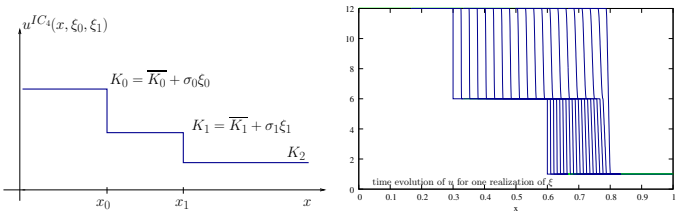

Fig. 1. Initializations for test-case IC_3 (left) and time evolution of the solution for one realization of the random variables: the second shock reaches the first one whatever the realization of the random variables and absorbs is (right).

Note that the solution at this time and location obtained from the classical intrusive approach (or IPMM with $\theta(u) = \frac{u^2}{2}$) presents some oscillations in the stochastic space due to Gibbs phenomenon, see figure 2 (right).

Let's now apply our coupling approach: for the considered test-case, the non–truncated system, for $x \in \mathcal{D}\backslash\mathcal{D}_N$, is solved with a Monte-Carlo method with $N = 20000$ points and using $P_{high} = 8$. The truncated system is solved, for $x \in \mathcal{D}_N$ by applying sG-gPC (or IPMM with $\theta(u) = \frac{u^2}{2}$, see [27, 25]) with $P_{low} = 2$. The numerical scheme used for the discretization of the truncated system is the Roe scheme presented in [27]. The numerical scheme used for the discretization of the non trucated system is a classical Roe scheme.

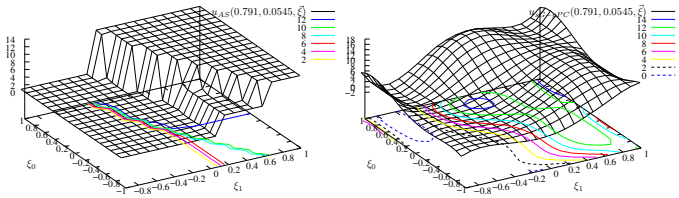

Fig. 2. Response surface results at time $t = 0.0545$ and position $x = 0.791$. Analytical solution (left), sG-gPC (= IPMM with $\theta(u) = \frac{u^2}{2}$) (right). The oscillations of the sG-gPC solution are due to Gibbs phenomenon.

Figure 3 (top-left) shows the initial condition of the mean with the initial condition for h: initially, only four cells of the physical space are not a equilibrium. These cells correspond to cells in the vicinities of the two initial discontinuities. The top right and bottom left figures of 3 shows these same quantities at two different times. For both figures, the non–truncated system's resolution area (Monte-Carlo) is in the vicinity of the moving discontinuities. In the smooth areas, the truncated system is solved (sG-gPC = IPMM with $\theta(u) = \frac{u^2}{2}$). The bottom right picture shows function $(\xi_0, \xi_1) \longmapsto u(0.791, 0.054, \xi_0, \xi_1)$, solution in the stochastic domain at fixed x and t. At these position and time, the truncated system is solved: the figure presents the solution in the stochastic space obtained with

[5] Three different: non–truncated/truncated, truncated/truncated and non–truncated/ non–truncated.

[6] Only in the case non–truncated/ truncated, the number of possibilities is very important. For example, we can choose

(i) MC / IPMM with entropy $\theta(u) = \frac{u^2}{2}$,
(ii) MC / IPMM with entropy $\theta(u) = s(u)$ where s is a mathematical entropy for the considered non–truncated system, see [27].
(iii) SPM / IPMM ...

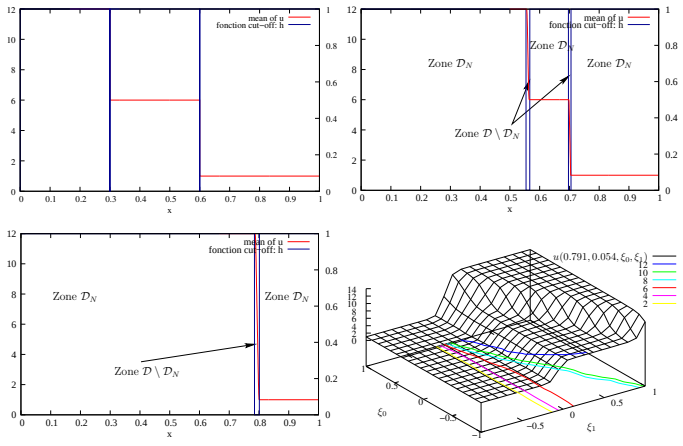

Fig. 3. Burgers test-case in two stochastic dimensions (cf. [27]) solved by the coupling method. The top left picture presents the initial conditions for the mean of u and for the function h. The top right and bottom left pictures shows these latter distributions at two different times. The non–truncated system, for $x \in \mathcal{D} \setminus \mathcal{D}_N$ is solved with with a MC method with $N = 20000$ points and using $P_{high} = 8$. The truncated system is solved, for $x \in \mathcal{D}_N$ by applying sG-gPC (or IPMM with $\theta(u) = \frac{u^2}{2}$, see [27, 25]) with $P_{low} = 2$. The physical discretization has 1000 cells. The bottom right picture shows the solution in the stochastic space at fixed $x = 0.791, t = 0.054$: at these position and time, the non–truncated system is solved and the solution at the points (20000 MC points) do not experience Gibbs phenomena.

the N realisations (Monte-Carlo). The use of the Monte Carlo method enables to avoid the appearance of Gibbs phenomenon in the vicinity of the discontinuities and to preserve a maximum principle (this is also the case in [13]).

The main advantage of coupling the MC and PC methods remains in its low cost compared to a classical Monte-Carlo approach on the whole domain together with its versatility and easiness toward the treatment of nonlinearities (no Gibbs phenomenon). Of course, the accuracy of the solution on the whole simulation domain, is dictated by the less accurate method: in this case, the MC approach (which converges slower than the PC approach). Table 2 shows the costs of the non-intrusive, coupling non-intrusive/intrusive and intrusive methods for the different considered problems. The methods are compared for equal characteristics in the different domains [7] but the **same accuracy** is obtain on the mean of u with the full MC approach and the coupling approach.

For Burgers' problem, the computational cost of the coupling method is almost the same as the one for the intrusive method (ratio of 1.01 between the CPU times, cf. table 2). It is much less important than the CPU cost of the full MC method. The CPU time of the coupling method is very close to the CPU time of the intrusive method because the non equilibrium area are very localized (few cells amongst the cells of the whole domain). For Euler system, the conclusion are quite different due to the expansion of the non linear domains, see next section.

Remark 3.1.1 *The coupling method is not conservative: the resolution errors for the different types of systems are not compensating. However, we have experimentally noticed that the more the physical and the stochastic spaces are refined, the less the conservativity error.*

3.2. *Compressible gas dynamics*

The methodology of section 2.4.1 is now applied to one-dimensional compressible flows modeled by Euler system:

$$\begin{cases} \partial_t \rho + \partial_x \rho u = 0, \\ \partial_t \rho u + \partial_x \rho u^2 + p = 0, \\ \partial_t \rho u + \partial_x \rho u e + p u = 0, \end{cases} \tag{22}$$

where ρ is the mass density, u is the velocity, e is the total energy and p is the pressure with perfect gas closure [8] $p = (\gamma - 1)\rho\epsilon$ with internal energy $\epsilon = e - \frac{u^2}{2}$.

First, a stochastic Riemann problem (Sod shock tube) uncertain initial condition is presented in subsection 3.2.1. Then a stochastic Richtmyer-Meshkov like problem with uncertain initial condition is studied in subsection 3.2.2. For more details about the test-cases, we refer to [27, 25].

In this section, we show the capacity of the method to couple two non-intrusive methods on each sides of the interface separating the equilibrium and non equilibrium domains. For $x \in \mathcal{D}_N$, the non–truncated system is solved by a MC method with N. For $x \in \mathcal{D} \setminus \mathcal{D}_N$, we solve the non–truncated system but with a SPM method with N_q and $N_q << N$. The coupling between the subdomains is done through polynomial reconstruction at the boundaries: the truncation orders are P_{low} at the boundaries at equilibrium and P_{high} at the boundaries of non equilibrium domains.

We chose to apply this non-intrusive / non-intrusive coupling to Euler system (rather than Burgers) because of the difficulty to develop numerical schemes for the truncated Euler system: in this case, the same numerical scheme is used in both domain: this puts forward one more advantage of the coupling approach.

3.2.1. *Sod shock tube*

This test-case is a stochastic Riemann problem with uncertain initial interface position: at $t = 0$, two fluids at rest are separated by an uncertain interface whose position is modeled by a uniform random variable $x_{interface} = 0.5 + 0.05\Xi$ where Ξ is uniform on $[-1, 1]$, see figure 4 (left) for the intial conditions on the mean and standard deviation of the mass density ρ. The initial condition are

[7] Number of points of the non-intrusive method and truncature order of the intrusive one etc.

[8] In practice, we took $\gamma = 1.4$ on the whole domain.

$$\begin{cases} \rho(x,0,\Xi) &= \begin{cases} 1 \text{ if } x \le x_{interface}(\Xi) \\ 0.125 \text{ otherwise} \end{cases}, \\ \rho u(x,0,\Xi) &= 0, \\ \rho e(x,0,\Xi) &= \begin{cases} 2.5 \text{ if } x \le x_{interface}(\Xi) \\ 0.25 \text{ otherwise.} \end{cases} \end{cases}$$

For one realization of the uncertain interface, three waves are propagating in the fluids: the left wave is a rarefaction fan in the heavy fluid, the second wave is an interface (contact discontinuity) and the right wave is a shock propagating in the light fluid. At time $t = 0.14$, the solution presents three area of important variability (non zero standard deviation) corresponding the area of the propagating waves (rarefaction, interface, shock, see figure 4 (right)).

3.2.2. *Richtmyer-Meshkov (RM) like shock tube*

For this test case, two fluids are separated by an stable interface. The light fluid (right of the interface) is shocked: as time passes, a shock will propagate toward the uncertain interface whose position is once again modeled by a uniform random variable $x_{interface} = 0.5+0.05\Xi$ where Ξ is uniform on $[-1, 1]$. Figure 4 (bottom left) shows the initial mean and standard deviation of the mass density with respect to x.

The full initial conditions are given by:

$$\begin{cases} \rho(x,0,\Xi) &= \begin{cases} 4, & \text{if } x \le x_{interf}(\Xi). \\ 1, & \text{if } x_{interf}(\Xi) \le x \le x_{shock}. \\ \dfrac{2\gamma - \gamma s + s}{2\gamma - \gamma s - s}, & \text{if } x \ge x_{shock}. \end{cases} \\ u(x,0,\Xi) &= \begin{cases} 0, & \text{if } x \le x_{interf}(\Xi). \\ 0, & \text{if } x_{interf}(\Xi) \le x \le x_{shock}. \\ -\sqrt{\dfrac{s(\rho-1)}{\rho(1-s)}}, & \text{if } x \ge x_{shock}. \end{cases} \\ p(x,0,\Xi) &= \begin{cases} 1, & \text{if } x \le x_{interf}(\Xi). \\ 1, & \text{if } x_{interf}(\Xi) \le x \le x_{shock}. \\ \dfrac{1}{1-s}, & \text{if } x \ge x_{shock}. \end{cases} \end{cases} \quad (23)$$

In this paper, we take $s = 0.5$ (strength of the shock wave hitting the uncertain interface), $\gamma = 1.4$, and $x_{shock} = 0.7$. Figure 4 (bottom right) shows the solution at time $T_{final} = 0.34$.

This test-case is relevant because when the shock hits the uncertain interface, the amplitude of the interface increases leading to a crash of classical intrusive codes (negative mass density in the stochastic space). From this latter interaction, three waves are propagating: one transmitted shock (left), one interface and one reflected shock. Once again, the uncertainty (non zero standard deviation) will be shared between these three waves as time passes, see figure 4 (bottom right).

3.2.3. *Interpretations and remarks*

In this section, we show the capacity of the method to couple two non-intrusive methods on each sides of the interface separating the equilibrium and non equilibrium domains. For $x \in \mathcal{D}_N$, the non–truncated system is solved by a MC method with $N = 20000$. For $x \in \mathcal{D} \backslash \mathcal{D}_N$, we solve the non–truncated system but with a SPM method with $N_q = 9$ (level 3 in Clenshaw-Curtis quadrature rule) so that we can consider $N_q << N$. The coupling between the subdomains is done through polynomial reconstruction at the boundaries: the truncation orders are $P_{low} = 3$ at the boundaries at equilibrium and $P_{high} = 8$ at the boundaries of non equilibrium domains. The simulations have 1000 cells and the numerical scheme is the Lagrange+Remap presented in [26, 19], with order $N_{\text{scheme}} = 3$. Figure 4 shows means,

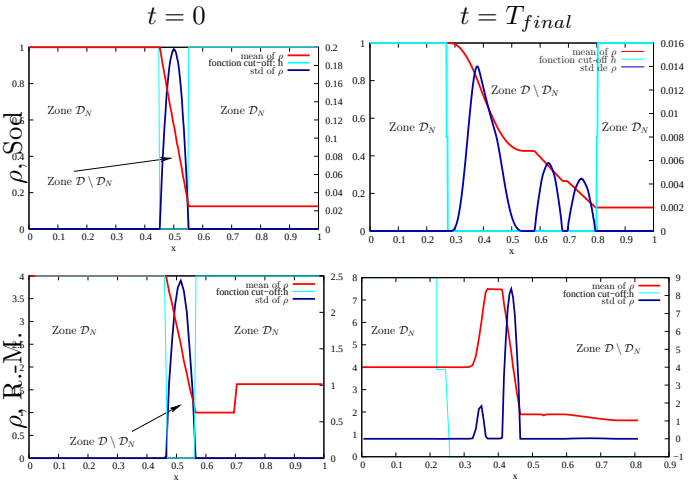

Fig. 4. Sod and 1–D Richtmyer-Meshkov–like stochastic test–cases: resolution by coupling non–truncated/non–truncated systems. For both test–cases, the uncertainty is carried by the initial condition: on the initial interface position modeled by a uniform random variable $x_{interface}(\Xi) = 0.5 + 0.05\Xi$. For $x \in \mathcal{D}_N$, the non–truncated system is solved by a SPM method with 1-D Clenshaw-Curtis rule of level 3 (i.e. 9 points). For $x \in \mathcal{D} \setminus \mathcal{D}_N$, we also solve the non–truncated system but with a MC method with 500 points. The truncation orders are $P_{low} = 3$ at equilibrium and $P_{high} = 8$ elsewhere. The simulations have 200 cells.

standard deviations (std) of the mass density with function h at initial and final times for both considered test-cases (Sod $T_f = 0.14$ (top) and Richtmyer-Meshkov $T_f = 0.34$ (bottom)). Initially, the non equilibrium areas are located in the vicinities of the interfaces, in the physical areas where the solutions present discontinuities in the stochastic space: in these areas, $h(x) = 0$ for both test-cases.

The right column shows the results at final times. For both simulations, the resolution areas of the non equilibrium system are spread to more than the half of the physical domain, contrary to the Burgers' results for which it remains very localized. Indeed, for the RM problem, the whole right side of the domain is $\mathcal{D} \setminus \mathcal{D}_N$. This is due to less localized nonlinear phenomenons classical of computational gas dynamics.

Remark 3.2.1 *Note that this emphasizes one more difficulty arising when dealing with nonlinear systems: the nonlinearity quickly propagates through the resolution domain and the area of importance (in the sense where the computation are costful and need accuracy) grows fast.*

Nevertheless, even in this case of spreading non equilibrium zones, the coupling approach remain competitive in term of computational cost, see table 2.

	Full MC (1)	Coupling (2)	full PC (3)	$\frac{(1)}{(2)}$	$\frac{(2)}{(3)}$
Burgers	16731.03 s.	1274.74 s.	1108.68 s.	13.13	1.14
Sod	465 s.	135 s.	3 s.*	6.37	13.2
R.-M. 1-D	30 mn 27 s.	11 mn 14 s.	55 s.*	3.44	45

Table 2
CPU times for the different stochastic problems (Burgers, Sod, 1-D Richtmyer-Meshkov) for three uncertainty propagation methods: non-intrusive, coupling intrusive/intrusive (or non-intrusive/non-intrusive for Euler) and intrusive. The methods are compared for equal polynomial orders and/or number of points recalled in the latter respective sections. The results presenting * recall that the sG-gPC method (IPMM with $\theta = \frac{u^2}{2}$) could not have been used (negative mass density and crash of the intrusive code): the SPM method with 9 points 1-D Clenshaw-Curtis rules has been used instead even if not really representative (as the same accuracy is not reached with (3) for the three problems. The red color for (1), (2) recalls that these CPU times have been obtained for simulations, full MC and coupling method, having the same accuracy (the (3) being less accurate but having the same parameter as in the equilibrium domain).

Figure 5 shows the RM computation at two later times and emphasizes the capability of the coupling approach to follow the non equilibrium areas: the boundary conditions are: wall type on the left and neutral on the right so that the transmitted shock reflects on the wall and hit back the interface resulting in one more transmitted (leaving the interface and going to the right) and one more reflected (leaving the interface and going toward the wall) shock.

In the Euler cases, the coupling method ensures a CPU time gain in comparison with the non-intrusive method (table 2). However, it remains more costful than the intrusive method: this can be explained by the fact that for Burgers' equation, the non equilibrium areas are very localized, which is not the case for Euler system. The coupling approach still present some advantages, even in the Euler case: it is transparent to the negative mass density problems (Gibbs), negative pressure etc. emphasized in [27, 25] and to nonlinearities.

Remark 3.2.2 *According to these results, the coupling of intrusive ($\theta(u) = \frac{u^2}{2}$) / intrusive ($\theta(u) = s(u)$)[9] seems encouraging: indeed, the IPMM approach with proper entropy closure reveals to be more accurate than sG-gPC in nonlinear areas (see [27]) but needs a additional step in the resolution (minimization algorithm). The use of sG-gPC in equilibrium areas and IPMM $\theta = s$ is non equilibrium ones could consequently reduce the cost of IPMM $\theta = s$. This will be investigated in further publications.*

[9] where s is the mathematical entropy.

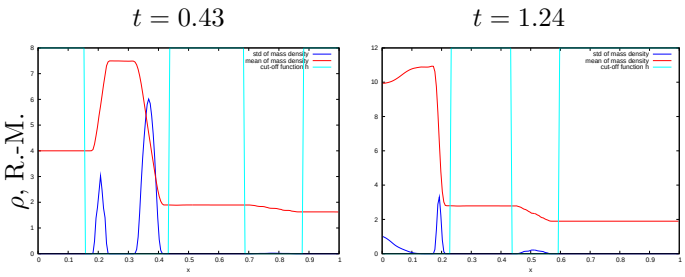

Fig. 5. Same simulation as described in susbsection 3.2.2, with the same parameters as in figure 5 but for more advanced times. The left picture shows the behavior of the heuristic with time: at $t = 0.43$, the non equilibrium area is non connex anymore (two non equilibrium areas, one in the vicinity of the transmitted shock and interface and one other in the vicinity of the reflected shock. The transmitted shock then hits the left wall and reflects to go back in the direction of the interface: at $t = 1.24$ (right picture), the two non equilibrium areas are in the vicinity of the interface and the reflections between the wall and interface of the first transmitted shock and in the vicinity of the second transmitted shock which went through the interface and propagates toward the right boundary.

Note that the CPU times for the fully intrusivelly solved Euler system have been obtained by application of IPMM with $\theta = s$ with s the mathematical entropy of the Euler system (see [27]) as in the case $\theta = \frac{u^2}{2}$ (sG-gPC), the code crashes due to numerical instabilities triggered by Gibbs phenomena, [27, 25].

4. Summary

In this paper, we have presented a new adaptive uncertainty propagation methods based on the resolution of different systems in different parts of the *physical* domain, rather than the stochastic one. The approach is based on an analogy with kinetic/moment theory and inspired by methods developed for coupling Boltzmann equation with the Euler system.

The coupling method suggested in this paper enables to solve the truncated system in equilibrium areas, smooth solution areas, and the non–truncated system elsewhere (presence of discontinuities or steep/stiff gradient). The method combines the advantages of both uncertainty propagation methods: indeed, in smooth areas, the exponential convergence is ensured. In the non smooth areas, the use of a non-intrusive method stabilizes the solver and avoids the appearance of the Gibbs phenomena. Moreover, its implementation is completely transparent to nonlinear effects.

In certain particular cases, the method enables an important gain in the CPU time (e.g. in the case of localized non linear phenomenon). At the present time, the method seems more costful than a purely intrusive approach but is clearly cheaper than a purely non-intrusive method.

The method implies the use of an arbitrary criteria characterizing the different physical subdomains in which are solved the different systems. The criteria used in this paper has been chosen for its simplicity and is quite constraining: a more in depth study of the effect of this criteria will be tackled in further publications. Note that the method do not need the tracking of discontinuities in the stochastic space (as usual adaptive UQ methods do, see [34, 1, 21]): the adaptation only rely on a decomposition of the *physical* domain.

The method enables to choice of the stochastic resolution methods in the different parts of the domain: many combinations are possible [10] and will be studied later on. In this paper, we focused on one combination implying the coupling of the truncated and the non–truncated system, leading to two combinations for the resolution methods: IPMM [11] ($\theta(u) = \frac{u^2}{2}$) with MC [12] for Burgers' equation and SPM [13] with MC [14]. Note that the coupling described is also independent of the physical solvers, i.e. different numerical schemes in the different resolution domains can be used.

[10] SPM/IPMM , MC/IPMM, SPM/SPM, IPMM/IPMM, etc.
[11] for the truncated system.
[12] for the non–truncated system.
[13] for the truncated system.
[14] for the non–truncated system.

References

[1] R. Abgrall. A Simple, Flexible and Generic Deterministic Approach to Uncertainty Quantifications in Non Linear Problems: Application to Fluid Flow Problems. *Rapport de Recherche INRIA*, 2007.

[2] R. Archibald, A. Gelb, R. Saxena, and D. Xiu. Discontinuity Detection in Multivariate Space for Stochastic Simulations. *J. Comp. Phys.*, 228(7):2676–2689, 2009.

[3] Boutin B., Chalons C., and Raviart P.-A. Existence result for the coupling problem of two scalar conservation laws with riemann initial data. *Math. Models Methods Appl. Sci.*, 2010. To appear.

[4] J. B. Bell, J. Foo, and A. L. Garcia. Algorithm Refinement for the Stochastic Burgers' Equation. *J. Comp. Phys.*, 223:451–468, 2007.

[5] M. Bieri and C. Schwab. Sparse high order FEM for elliptic sPDEs. *Computer Methods in Applied Mechanics and Engineering*, 198(13-14):1149 – 1170, 2009. HOFEM07 - International Workshop on High-Order Finite Element Methods, 2007.

[6] G. Blatman and B. Sudret. Sparse polynomial chaos expansions and adaptive stochastic finite elements using a regression approach. *Comptes Rendus Mécanique*, 336(6):518 – 523, 2008.

[7] Benjamin Boutin. *Mémoire de thèse de doctorat, Étude mathématique et numérique d'équations hyperboliques non-linéaires : couplage de modèles et chocs non classiques.* PhD thesis, Universit Pierre et Marie Curie, Paris 6, 2009. http://tel.archives-ouvertes.fr/tel-00437289/fr/.

[8] S. Boyaval, C. Le Bris, Y. Maday, N. C. Nguyen, and A. T. Patera. A reduced basis approach for variational problems with stochastic parameters: Application to heat conduction with variable Robin coefficient. *Computer Methods in Applied Mechanics and Engineering*, 198(41-44):3187 – 3206, 2009.

[9] J.-C. Chassaing and D. Lucor. Numerical investigation of airfoil performance at stochastic transonic flow regimes. 5th ECCOMAS Conference, 30 June - 4 July, 2008.

[10] J.-C. Chassaing and D. Lucor. Stochastic investigation of flows about airfoils at transonic speeds. *AIAA J.*, 48(5):in press, May 2010.

[11] G. Chen, C. Levermore, and T. Liu. Hyperbolic Conservation Laws with Stiff Relaxation Terms and Entropy. *Comm. Pure Appl. Math.*, 47:787–830, 1994.

[12] P. G. Constantine, A. Doostan, and G. Iaccarino. A hybrid collocation/Galerkin scheme for convective heat transfer problems with stochastic boundary conditions. *International Journal for Numerical Methods in Engineering*, 80(6-7):868–880, 2009.

[13] P. Degond, G. Dimarco, and L. Mieussens. A Moving Interface Method for Dynamic Kinetic-Fluid Coupling. *J. Comp. Phys.*, 227(10):1176–1208, 2007.

[14] P. Degond, S. Jin, and L. Mieussens. A Smooth Transition Model between Kinetic and Hydrodynamic Equations. *J. Comp. Phys.*, 209:665–694, 2005.

[15] Tammo Dijkema, Christoph Schwab, and Rob Stevenson. An adaptive wavelet method for solving high-dimensional elliptic PDEs. *Constructive Approximation*, 30(3):423–455, 12 2009.

[16] Jasmine Foo and George Em Karniadakis. Multi-element probabilistic collocation method in high dimensions. *Journal of Computational Physics*, 229(5):1536–1557, 2010.

[17] R. Ghanem. Hybrid stochastic finite elements and generalized Monte Carlo simulation. *Journal of Applied Mechanics*, 65(4):1004–1009, 1998.

[18] R.G. Ghanem and P. Spanos. *Stochastic Finite Elements: a Spectral Approach*. Springer-Verlag, 1991.

[19] H. Jourdren and S. Del Pino. Arbitrary High-Order Schemes for the Linear Advection and Wave Equations: Application to Hydrodynamics and Aeroacoustics. *C.R. Acad. Sci. paris, Ser. I*, 342:441–446, 2006.

[20] J. Le Meitour, D. Lucor, and J.-C. Chassaing. Prediction of stochastic limit cycle oscillations using an adaptive Polynomial Chaos method. *Journal of Aeroelasticity and Structural Designs*, 2(1):3–22, 2010.

[21] O. P. Le Maître and O. M. Knio. Uncertainty Propagation using Wiener-Haar Expansions. *J. Comp. Phys.*, 197:28–57, 2004.

[22] L. Mathelin and O. P. Le Maître. A Posteriori Error Analysis for Stochastic Finite Element Solutions of Fluid Flows with Parametric Uncertainties. *ECCOMAS CFD*, 2006.

[23] I. Müller and T. Ruggeri. *Rational Extended Thermodynamics, 2nd ed.* Springer. Tracts in Natural Philosophy, Volume 37, 1998. Springer-Verlag, New York.

[24] F. Nobile, R. Tempone, and C. Webster. A Sparse Grid Stochastic Collocation Method for Partial Differential Equations with Random Input Data. *SIAM J. Numer. Anal.*, 46(5):2309–2345, 2008.

[25] G. Poëtte. *Propagation d'Incertitudes pour les Systèmes de Lois de Conservation, Méthodes Spectrales Stochastiques*. Phd thesis, Université Pierre et Marie Curie, Institut Jean Le Rond D'Alembert, 2009.

[26] G. Poëtte, B. Després, and D. Lucor. Treatment of Uncertain Interfaces in Compressible Flows. *Comp. Meth. Appl. Math. Engrg.*, 2009. Submitted.

[27] G. Poëtte, B. Després, and D. Lucor. Uncertainty Quantification for Systems of Conservation Laws. *J. Comp. Phys.*, 228(7):2443–2467, 2009.

[28] G. Poëtte, D. Lucor, and B. Després. Uncertainty Propagation for Systems of Conservation Laws, High-Order Stochastic Spectral Methods. In Springer, editor, *International Conference On Spectral Analysis and High Order Methods*, 2009.

[29] F. Simon, P. Guillen, P. Sagaut, and D. Lucor. A gPC-based approach to uncertain transonic aerodynamics. *Computer Methods in Applied Mechanics and Engineering*, 199:1091–1099, 2010.

[30] P. Le Tallec, J.-F. Bourgat, and M. D. Tidriri. Coupling Boltzmann and Navier-Stokes Equations by Friction. *J. Comp. Phys.*, 127:127–245, 1996.

[31] P. Le Tallec and F. Mallinger. Coupling Boltzmann and Navier-Stokes Equations by Half Fluxes. *J. Comp. Phys.*, 136:51–67, 1997.

[32] X. Wan and G.E. Karniadakis. An adaptive multi-element generalized polynomial chaos method for stochastic differential equations. *Journal of Computational Physics*, 209:617–642, 2005.

[33] X. Wan and G.E. Karniadakis. Long-term behavior of polynomial chaos in stochastic flow simulations. *Computer Methods in Applied Mechanics and Engineering*, 195:5582–5596, 2006.

[34] X. Wan and G.E. Karniadakis. Multi-Element generalized Polynomial Chaos for Arbitrary Probability Measures. *SIAM J. Sci. Comp.*, 28(3):901–928, 2006.

[35] N. Wiener. The Homogeneous Chaos. *Amer. J. Math.*, 60:897–936, 1938.

for $x \in \mathcal{D}_N, \varepsilon^P \nrightarrow 0$	for $x \in \mathcal{D} \backslash \mathcal{D}_N$, $\varepsilon^P \longrightarrow 0$
non–truncated system	$P-$**truncated system**
$\partial_t u_G^{\varepsilon^P} + h\partial_x f(u_G^{\varepsilon^P} + u_{eq}^P) = 0$	$\partial_t U_D^{\varepsilon^P} + (1-h)\partial_x \left[\int f(u_{eq}^P + u_G^{\varepsilon}) \Phi \mathrm{d}\mathcal{P} \right] = 0$
Numerical resolution methods	
non-intrusive (MC, SPM,...)	**Intrusive** (sG-gPC, IPMM, SPM, ME-gPC,...)
Choice of N points $(\xi_i)_{i\in\{1,...,N\}}$ of weights $(w_i)_{i\in\{1,...,N\}}$	Choice of the basis $(\phi_0, ..., \phi_P)^t$, of the closure entropy $\theta(u)$
$\{(\varepsilon^P \nrightarrow 0) \Longrightarrow h(x) = 1\}$ $\Downarrow$	$\{(\varepsilon^P \longrightarrow 0) \Longrightarrow h(x) = 0\}$ $\Downarrow$
$\left\{ \begin{array}{c} \partial_t u_G^{\varepsilon^P}(x,t,\xi_0) + \partial_x f(u_G^{\varepsilon^P}(x,t,\xi_0)) = 0, \\ \partial_t u_G^{\varepsilon^P}(x,t,\xi_1) + \partial_x f(u_G^{\varepsilon^P}(x,t,\xi_1)) = 0, \\ \cdots, \end{array} \right.$	$\partial_t U_D + \partial_x \int f(u_{eq}^P) \begin{pmatrix} \phi_0 \\ \cdots \\ \phi_P \end{pmatrix} \mathrm{d}\mathcal{P} = 0$
Boundary conditions between domains for fixed t	
In $\partial(\mathcal{D} \setminus \mathcal{D}_N)$: moments on boundary	In $\partial\mathcal{D}_N$: values on boundary
$u_G^{\varepsilon^P}(x,t,\xi_i)$ known $\forall i \in \{1,...,N\}$ $\Downarrow$ $\left\{ \begin{array}{c} u_k^{Bords}(x,t) \approx \sum_{i=1}^{N} w_i u_G^{\varepsilon^P}(x,t,\xi_i)\phi_k(\xi_i) \\ \text{known } \forall k \in \{0,\ldots,P\} \end{array} \right\}$	$u_k(x,t)$ known $\forall k \in \{0,..,P\}$ $\Downarrow$ $\left\{ \begin{array}{c} u_{eq}^P(x,t,\xi_i) = \nabla_\lambda \theta^*(\Pi^P \lambda(x,t,\xi_i)) \\ \text{known } \forall i \in \{0,...,N\} \end{array} \right\}$

Table 1
Description of the coupling algorithm for the resolution of non–truncated/truncated subsystems. The coupling is effective through imposing correct boundary conditions between the different regions.